and, therefore

$$f_A(\lambda) = n_{DU}[5.195 \exp(-1.77\lambda n_{DU}) + 45.916 \exp(-3.32\lambda n_{DU})] \quad (23)$$

The probability of failure according to Eq. (15) with $F_Z(\lambda)$ from Eq. (16)

$$p_f = n_{DU} \int_0^1 \left\{1 - \exp\left[-\left(-\frac{ln\omega}{0.96}\right)^{19}\right]\right\} \times [5.195\omega^{(1.77nDU^{-1})} + 45.916\omega^{(3.32nDU^{-1})}]d\omega \quad (24)$$

where $\omega = \exp(-\lambda)$.

Equation (24) has been numerically evaluated for the ultimate design load factors n_{DU} = 13, 11, 9, and 7 and the corresponding reliability functions have been constructed in accordance with Eq. (14) and are represented in Fig. 8 in terms of the number of load cycles and of hours of flight. The conversion is based on the assumption that roughly 10^2 load cycles are equivalent to 1 hr of flight at an average of 350–400 mph in accordance with the flight records.

References

[1] Jablecki, L. S., *Analysis of the Premature Structural Failures in Static Tested Aircraft*, Verlag Leemann, Zurich, 1955, pp. 11 and 25.

[2] Freudenthal, A. M., "Safety and the Probability of Structural Failure," *Transactions of the American Society of Civil Engineers*, Vol. 121, 1956, pp. 1337–1397; also "Safety, Reliability and Structural Design," *Journal Structural Division, Proceedings of the American Society of Civil Engineers*, Vol. 92, 1961. "The Analysis of Structural Safety," *Journal of the Structural Division, Proceedings of the American Society of Civil Engineers*, Vol. 92, No. ST 1, Paper 4682, Feb. 1966, p. 283.

[3] Gumbel, E. J., *Statistics of Extremes*, Columbia University Press, New York, 1958, p. 281.

[4] McCulloch, A. J., "Development of Fatigue Loading Spectra for Testing Aircraft Components and Structures," *Symposium on Fatigue of Aircraft Structures*, Special Tech. Publication No. 274, 1960, American Society for Testing Materials, p. 36.

[5] McDougal, R. L., Colemann, T. L., and Smith, P. L., "The Variation of Atmospheric Turbulence with Altitude and its Effect on Airplane Gust Loads," RM L53G15A, 1953, NASA.

[6] Hoblit, F. M. et al., "Development of a Power Spectral Gust Design Procedure for Civil Aircraft," Rept. FAA-ADS-53, Jan. 1966, Federal Aviation Agency.

[7] Vahldiek, A. M., "Maneuver Load Data from F-105B Aircraft," ASD-TN-61-161, 1961; "Structural Flight Loads Data from F-106A Aircraft," ASD-TDR-62-246, 1962, Flight Dynamics Lab., Wright Patterson Air Force Base.

MAY-JUNE 1970 J. AIRCRAFT VOL. 7, NO. 3

Response of Complex Structures to Turbulent Boundary Layers

LOYD D. JACOBS,* DENNIS R. LAGERQUIST,† AND FRED L. GLOYNA‡

The Boeing Company, Renton, Wash.

A turbulent boundary-layer loading function is developed for use with a finite-element structural analysis system and applied in a study of the random vibration of elastic aircraft structures. The method is demonstrated by computing the random vibration response of simple and complex structures; the method is evaluated by comparing computed and measured response on the simple panel. Deflection cross-power spectral density and deflection covariance are the criteria used to compare panel response. The simple panels are flat and clamped. The complex panels are flat and curved fuselage sections: 1) skin panels with tear straps and 2) six stringers attached to a skin strip. The effects of fuselage radius and of static in-plane loads due either to cabin pressurization or flight loads are discussed. The influence of boundary-layer thickness on the size of the region of coherent structural response is also discussed.

Nomenclature

$[A]$ = diagonal matrix of elemental areas on structure
A_i, A_j = elemental area on structure associated with i and j node points, in.^{2}
A_n = const, $A_1 = 12.0$, $A_2 = 7.20$, $A_3 = 1.58$
B = $1/0.8\delta^*$, in.$^{-1}$
$[C]$ = damping matrix
$C_{F_{ij}}(\omega)$ = force co-power spectral density (co-PSD) acting on plate pairs i and j, lb^2·sec
$[C_F(\omega)]$ = force co-power spectral density matrix, lb^2·sec
$[C_\delta(\omega)]$ = deflection co-power spectral desity matrix, in.^{2}·sec
$[H(i\omega)]$ = complex frequency response matrix
$[K]$ = stiffness matrix
K^2 = normalization constant for power spectral density defined by $K^2 = \langle p^2 \rangle / \tau_w^2 = \sum_{n=1}^{3} A_n/K_n$
K_n = const, $K_1 = 13.9$, $K_2 = 2.94$, $K_3 = 0.471$
M = Mach number
$[M]$ = diagonal mass matrix
$Q_{F_{ij}}(\omega)$ = force quad-power spectral density acting on plate pairs i and j, lb^2·sec
$[Q_F(\omega)]$ = force quad-power spectral density matrix, lb^2·sec
$R(\ )$ = real part of a complex number, function, or matrix
S = $\omega\delta^*/U$, Strouhal number, dimensionless frequency
U = freestream airflow velocity or aircraft speed, in./sec
U_c = convection velocity, in./sec

Received January 15, 1969; presented as Paper 69-20 at the AIAA 7th Aerospace Sciences Meeting, New York, January 20–22, 1969; revision received August 18, 1969. This work was supported in part by the U.S. Air Force Flight Dynamics Laboratory under Contract AF33(615)-5155. The computer programs developed for and used in this study were written by K. Tsurusaki and F. S. Wallace of The Boeing Company. We are indebted to R. C. Leibowitz, Naval Ship Research and Development Center, and M. C. Young, The Boeing Company, because their checking resulted in some corrections in the final boundary-layer loading equations.

* Research Specialist, Structures Research, Commercial Airplane Group. Member AIAA.

† Research Engineer, Structures Research, Commercial Airplane Group.

‡ Research Engineer, Acoustics Research, Commercial Airplane Group.

a = $1/U_c\theta$, in.$^{-1}$
b = ω/U_c, in.$^{-1}$
f = frequency, Hz
i = $(-1)^{1/2}$
i,j = finite element node points
m_{ij},n_{ij} = integers used to denote separation distance between the i and j node in x and y direction, respectively
$\tilde{p}$ = rms pressure fluctuation, $[\langle p^2\rangle]^{1/2}$, psi
$\langle p^2\rangle$ = mean square fluctuating pressure at the wall in turbulent boundary layer, psi^2
t = panel thickness, in.
x,y = Cartesian coordinates, in.
x_i,y_i = Cartesian coordinates of ith node point, in.
$\Phi_{F_{ii}}(\omega)$ = force power spectral density acting on the ith structural plate, lb^2·sec
$\Phi_{F_{ij}}(i\omega)$ = cross-power spectral density of forces acting on plate pair i and j, a complex function of ω, lb^2·sec
$[\Phi_F(i\omega)]$ = force cross-power spectral density matrix, lb^2·sec
δ^* = boundary-layer displacement thickness, in.
δ = rms displacement, in.
ζ = critical damping ratio
η = separation distance in y direction, in.
η_i,η_j = distance in y direction between node and dummy variable on ith and jth nodal areas, respectively, in.
η_0 = y-direction separation distance between adjacent nodes, in.
θ = eddy lifetime, sec
λ,μ = constants for stiffness and inertia proportional damping, respectively
ξ = separation distance in x direction, in.
ξ_i,ξ_j = distance in x direction between node and dummy variable on ith and jth nodal areas, respectively, in.
ξ_0 = smallest basic x-direction separation distance between adjacent nodes, in.
$\rho(\xi,\eta;\tau)$ = cross-correlation coefficient, $-1 \leq \rho(\xi,\eta;\tau) \leq +1$
τ = time delay, sec
$[\phi]$ = matrix of eigenvectors
$\{\phi^r\}$ = eigenvector column matrix
ω = angular frequency, $2\pi f$, rad/sec
ω_j = eigenfrequency of structure, modal frequency, rad/sec
$[\ ]^T$ = transpose of matrix
$(\ )^*$ = complex conjugate
$\langle\ \rangle$ = time average

Introduction

TURBULENT boundary layers attached to the exterior fuselage are a major source of passenger cabin noise during flight of subsonic aircraft. This noise is caused by the random vibration of the cabin structure responding to boundary-layer fluctuating pressures. The random fluctuating pressures result from turbulent velocity eddies in the boundary-layer region close to the skin. This paper develops a turbulent boundary-layer loading function for use with finite-element, structural systems. The method of response analysis and the resulting computer program are discussed. The loading function is then applied in a study of the boundary-layer induced random vibration of simple and complex structures simulating sections of aircraft fuselages. Emphasis is placed on the low-frequency response of structure where changes in structural design have major effects on response.

The problem of random vibration of linear, elastic, mechanical systems to ergodic stationary random loads has been discussed by Powell,[1] Eringen,[2] and Lyon.[3] These studies applied the methods of random process theory to mechanical systems. Others have taken these methods and worked example problems on the random vibration of simple structures. Thomson and Barton[4] calculated the response of a rod to a single-point random axial load on the rod end. Dyer[5] calculated response of a simply supported panel to a simplified turbulent boundary-layer model based on a decaying and convected rain-on-the-roof type load. Wilby[6] used a more accurate model for turbulent boundary-layer loads, and calculated and measured the response of single and multiple bays of simple skin panels. Trubert[7] demonstrated these methods on a complex cantilevered beam subjected to dual random loads, using experimentally determined admittance functions and load cross-power spectral densities to calculate random response. Trubert's work has been extended to distributed random loads applied to finite-element structural systems by Fuller and Newsom,[8] Newsom[9] alone, and Newsom, Fuller, and Sherrer.[10] This paper extends these methods to the small-scale distributed and convected random loading of the attached turbulent boundary layer.

Response Analysis Method

The method of response analysis is an extension of matrix structural analysis (finite-element) methods. Matrix methods for dynamic response are combined with random process theory to analyze structure subjected to random pressure loads. Jacobs and Lagerquist[11] give a comprehensive discussion of the response analysis method; thus, only the main features are summarized here.

Response to Random Pressure Loads

One statistical quantity useful for describing random processes is cross-power spectral density (cross-PSD). For ergodic stationary random processes, acting on a linear elastic structure, the relation between response cross-PSD and pressure-loading cross-PSD is

$$[\Phi_\delta(i\omega)] = [H^*(i\omega)][A][\Phi_p(i\omega)][A][H(i\omega)]^T \quad (1)$$

where $[\Phi_\delta(i\omega)]$ and $[\Phi_p(i\omega)]$ are cross-PSD matrices of displacement and pressure, respectively, $[H(i\omega)]$ is the admittance matrix, and $[A]$ is a diagonal matrix of areas associated with node points. The asterisk denotes the complex conjugate and $i\omega$ denotes complex functional dependence on ω. The diagonal elements of the left-hand matrix are displacement PSD. The off-diagonal terms are displacement cross-PSD terms. The cross-PSD matrices are hermitian, i.e., the matrix can be written as a sum of a real symmetric matrix (co-power spectral density) $[C(\omega)]$ and a real skew-symmetric matrix (quad-power spectral density) $[Q(\omega)]$ as follows.

$$[\Phi(i\omega)] = [C(\omega)] + i[Q(\omega)] \quad (2)$$

Admittance Matrix

The admittance matrix has the form

$$[H(i\omega)] = [-\omega^2[M] + i\omega[C] + [K]]^{-1} \quad (3)$$

where $[M]$, $[C]$, and $[K]$ are square matrices of inertia, viscous damping, and stiffness coefficients, respectively. The symmetric stiffness matrix $[K]$ can be determined from the displacement method of static matrix structural analysis techniques. Matrix $[M]$ is diagonal for a system of concentrated point masses.

Special Forms of Damping

For certain forms of damping, the admittance matrices are uncoupled when displacements are expressed in terms of a set of generalized coordinates based on normal mode shapes. This uncoupling results in diagonal admittance matrices when viscous damping is proportional to inertia, stiffness, or both. Let

$$[C] = \mu[M] + \lambda[K] \quad (4)$$

where μ and λ are proportionality factors. Then, the admittance matrix is

$$[\mathrm{H}(i\omega)] = [\phi][H_j(i\omega)][\phi]^T \quad (5)$$

where each column of $[\phi]$ is a normal mode $\{\phi^j\}$ and ω_j is the jth natural frequency. The term $H_j(i\omega)$ is the jth generalized

admittance defined by

$$H_j(i\omega) = 1/M_j(-\omega^2 + i\omega(\mu + \lambda\omega_j^2) + \omega_j^2) \quad (6)$$

The term M_j is the jth generalized mass defined by

$$M_j = \{\phi^i\}^T[M]\{\phi^i\} \quad (7)$$

It is often convenient to represent the damping as a fraction of critical damping. The modal damping factor ζ_j represents the fraction of critical damping in the jth mode (see Hurty and Rubinstein[12]). This factor is related to viscous damping proportionality factors μ and λ in Eq. (4) by the relationship

$$2\zeta_j = \mu/\omega_j + \lambda\omega_j \quad (8)$$

Deflection Response PSD

When damping does not couple the equations of motion, Eq. (1) can be simplified by using the generalized admittance matrix defined in Eq. (5). Then the displacement cross-PSD is a double summation over m modes.

$$[\Phi_\delta(i\omega)] = \sum_{j=1}^{m}\sum_{k=1}^{m} H_j^*(i\omega)H_k(i\omega)[\Phi_F{}^{ik}(i\omega)] \quad (9)$$

where

$$[\Phi_F{}^{ik}(i\omega)] = \{\phi^i\}\{\phi^i\}^T[\Phi_F(i\omega)]\{\phi^k\}\{\phi^k\}^T$$

and

$$[\Phi_F(i\omega)] = [A][\Phi_p(i\omega)][A]$$

For lightly damped systems with well separated natural frequencies, an approximate solution results by deleting cross-product terms, so that the double summation in Eq. (9) reduces to a single-summation approximation for deflection co-PSD

$$[C_\delta(\omega)] = \sum_{j=1}^{m} |H_j(i\omega)|^2[C_F{}^{jj}(\omega)] \quad (10)$$

These approximations lead to zero response quad-PSD. Hence, only $[C_\delta(\omega)]$ appears on the left and only the diagonal terms are used.

Deflection Covariance

The joint deflection moment for a structure can be obtained from integration of corresponding terms of deflection cross-PSD. All such terms can be considered at once and written as a matrix integration.

$$[\langle\delta_q\delta_r\rangle] = \int_0^\infty [C_\delta(\omega)]d\omega \quad (11)$$

The angular brackets denote a time average. The elements of $[\langle\delta_q\delta_r\rangle]$ are the covariances of all pairs of structural node points. The diagonal elements are mean square deflections, and the off-diagonal terms are time averages of products of deflections at different node points (space correlation).

When damping is in such a form that it causes the response equations to uncouple through use of normal modes, the matrix of joint deflection moments in Eq. (11) can be simplified as in Eq. (9). If, in addition, the rate of change of excitation force PSD is small about each region of high modal response, then the excitation force can be considered a constant evaluated at the set of frequencies ω_{jk} determined from the natural frequencies. Then, the deflection covariance matrix reduces to

$$[\langle\delta_q\delta_r\rangle] \simeq R\left\{\sum_{j=1}^{m}\sum_{k=1}^{m}[\Phi_F{}^{ik}(i\omega_{jk})]\int_0^\infty (H_j^*(i\omega)H_k(i\omega))d\omega\right\} \quad (12)$$

where

$$\omega_{jk} = (\omega_j + \omega_k)/2$$

The scalar integral of generalized admittance cross products has been evaluated and the results are summarized by Lagerquist and Jacobs.[13]

When damping is small, the double summation reduces to a single summation ($j = k$). When the integral of generalized admittances is evaluated with $j = k$, Eq. (12) reduces to

$$[\langle\delta_q\delta_r\rangle] \simeq \sum_{j=1}^{m}[C_F{}^{jj}(\omega_j)]\frac{\pi}{4M_j{}^2\omega_j{}^3\zeta_j} \quad (13)$$

A self-contained computer program described by Lagerquist and Jacobs[13] and Tsurusaki and Wallace[14] was used to perform structural response calculations. The program can obtain either the approximate solution based on Eq. (10) and Eq. (13) or make the more accurate and lengthy calculations based on Eqs. (9) and (12). Use of this computer program in sonic fatigue analysis is also discussed by Jacobs and Lagerquist.[15]

Turbulent Boundary-Layer Fluctuating Pressures

Fluctuating pressures in turbulent boundary layers have been studied on gliders, airplanes, missiles, scale models in wind tunnels, and in special boundary-layer channels.[16-27] The flow channel studies have been the most complete.

Maestrello[16,17] reports experimental results for fluctuating pressures in subsonic turbulent boundary layers measured in an open circuit flow channel. From these results, he has synthesized nondimensional models of pressure PSD and space-time correlation.

The normalized and dimensionless form of PSD of fluctuating wall pressures $\Pi(S)$ is

$$\Pi(S) = \frac{1}{K^2}\sum_{n=1}^{3} A_n e^{-K_n S} \quad (14)$$

where $S = \omega\delta^*/U$ (Strouhal number), a dimensionless frequency and K^2 is a normalization constant dependent upon constants A_n and K_n. Power in this spectrum is distributed over a large frequency range—three decades. Typically, for larger aircraft flying today, a Stouhal number of 10 corresponds to a frequency of 10 kHz and a Stouhal number of 10^{-2} corresponds to a frequency of 10 Hz. It is impossible to build an aircraft structure that does not have resonant response in this range.

Maestrello's normalized space-time correlation function ρ has the form

$$\rho(\xi,\eta;\tau) = \frac{e^{-|\tau|/\theta}}{K^2}\left\{\sum_{n=1}^{3}\frac{A_nK_n}{K_n{}^2 + B^2[(\xi - U_c\tau)^2 + \eta^2]}\right\} \quad (15)$$

where ξ is x direction and η is y direction separation distance between two pressure points, τ is delay time, $B = 1/0.8\delta^*$, δ^* is the boundary-layer displacement thickness, U_c is the mean eddy convection speed, and θ is mean eddy lifetime. The space-time correlation function depends on constants, decays with time delay, and has a convective form described by the term in brackets. As time delay increases, convection causes the point of maximum correlation to proceed downstream. This space-time correlation function defines an ergodic stationary and homogeneous random process. This model for the fluctuating wall pressure in the subsonic turbulent aerodynamic boundary layer is the starting point for developing a turbulent boundary-layer loading function for use with finite-element structural analysis systems.

Turbulent Boundary-Layer Loads

The statistical loading of the turbulent boundary-layer pressure fluctuations can conveniently be described by the cross-

PSD. Solutions of the response equations require this cross-PSD to be defined as a matrix compatible with structural finite-element methods. Definition of this boundary-layer loading function is summarized here; a more comprehensive treatment is given elsewhere by Jacobs and Lagerquist,[11] and Jacobs, Young, and Tsurusaki.[28]

Pressure PSD

The space-time correlation function can be transformed into the frequency domain by use of the Weiner-Khinchine relations,[29-31] which amounts to a Fourier transform

$$\Phi_p(\xi,\eta;i\omega) = \frac{\langle p^2\rangle}{\pi}\int_{-\infty}^{\infty} \rho(\xi,\eta;\tau)e^{-i\omega\tau}\,d\tau \qquad (16)$$

$$(0 < \omega < \infty)$$

where $\langle p^2\rangle$ is the mean square fluctuating pressure. The pressure cross-PSD $\Phi_p(\xi,\eta;i\omega)$ is a complex function. The results of this transformation are

$$\Phi_p(\xi,\eta;i\omega) = \frac{\langle p^2\rangle}{K^2BU_c}\, e^{-|\xi|/U_c\theta}\, e^{-i\omega\xi/U_c}\cdot \left\{\sum_{n=1}^{3}\frac{A_nK_ne^{-(\omega/BU_c)\,[K_n^2+B^2\eta^2]^{1/2}}}{[K_n^2+B^2\eta^2]^{1/2}}\right\} \qquad (17)$$

$$(0 < \omega < \infty)$$

where Taylor's hypothesis[32] has been used, making the integration possible. Taylor's hypothesis states that $|\tau|/\theta \simeq |\xi|/U_c\theta$. This hypothesis is a valid approximation for turbulent boundary-layer flow because fluctuating velocities are small when compared with total velocity, and changes of eddy patterns as they are convected from one point to another and decay are only slightly affected by time decay of the eddy.

The resulting pressure cross-power spectra shown in Fig. 1 decay slowly and oscillate in the flow direction ξ, and decay rapidly in the η direction normal to the direction of flow. Graphs of both co-power and quad-power spectral density are shown, the quad-spectra leading the co-spectra by 90°.

Force PSD

The problem in finite-element methods when used for solution of the response of structure subjected to boundary-layer noise is that there are many small pressure eddies over one finite element. A typical pressure eddy is shown in Fig. 2 being convected downstream with velocity U_c. As it progresses downstream it becomes diffused, loses strength and dissipates. The pressure eddy exerts incremental force over a small part of the total area associated with a node, called nodal area. There are many of these pressure eddies with various phase relationships over the panel, and each will exert an incremental force. The net force on the nodal area is desired. The normal method for determining forces on nodal areas has been to assume slowly varying pressure, so that pressure at the node point, when multiplied by nodal area, closely approximates total force. Obviously, in the case of the small-scale loads of a turbulent boundary layer, this method greatly overestimates the magnitude of total force. Net force must be determined by statistically adding incremental forces.

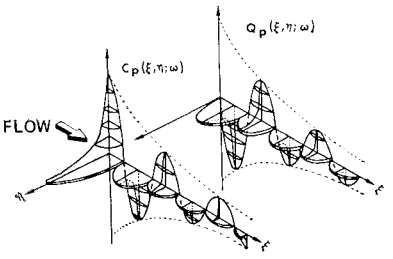

Fig. 1 Pressure cross - power spectra.

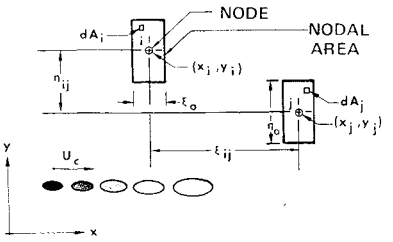

Fig. 2 Geometry of finite-plate elements.

Net force cross-PSD on nodes has been calculated by considering infinitesimal areas dA on pairs of node points with finite areas A. A pair of nodes i and j with nodal areas A_i and A_j are shown with infinitesimal areas dA_i and dA_j in Fig. 2. The infinitesimal areas are located at points (x'_i,y'_i) and (x'_j,y'_j), respectively. The infinitesimal force cross-PSD acting over areas dA_i and dA_j has been summed over the total area of the pair of nodes, determining the total force cross-PSD on the pair of nodes.

$$\Phi_{Fij}(i\omega) = \int_{A_i}\int_{A_j}\Phi_p[(x'_j - x'_i),\,(y'_j - y'_i);\,i\omega]dA_i\,dA_j \qquad (18)$$

$$\Phi_{Fij}(i\omega) = C_{Fij}(\omega) + iQ_{Fij}(\omega)$$

The equations resulting from this integration are summarized in the Appendix.

This then determines an element in the force cross-PSD matrix. When all these force cross-PSD terms for pairs of nodes are arranged to correspond to the ordering of terms in the structural stiffness matrix, the force co- and quad-power spectral density matrices are constructed per Eq. (2). The diagonal terms of the co-PSD matrix are the collection of force PSD at all node points. These diagonal terms are all equal because the turbulent boundary layer is approximately a homogeneous random process (its thickness changes very slowly within the distance of a structural panel). In addition, the $[\Phi_F(i\omega)]$ matrix is also hermitian.

Simple Panel in Duct Flow

In addition to fluctuating wall pressures, Maestrello[16,17] also reports on experimental measurements of simple panel response to turbulent boundary layers. The panel was inserted in the side of a small open circuit wind tunnel so that air flowed over the surface of the panel, exciting it and causing response. The panel and numbered points of deflection response measurement are shown in Fig. 3. The panel was constructed of 2024 aluminum alloy by machining the interior down from $\frac{3}{4}$-in. stock to varying thicknesses ranging from 0.020 to 0.080 in. Deflection response was calculated for Maestrello's 0.080-in.-thick panel by using the boundary-layer loading function and finite-element computer programs developed for random-vibration analysis. Calculated and measured results were compared as a check before applying the analysis method to more complex structures.

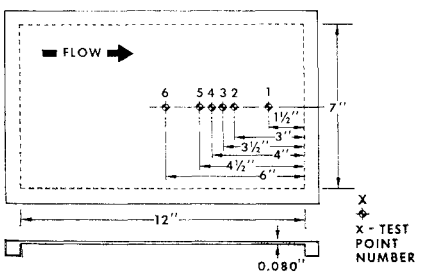

Fig. 3 Simple panel.

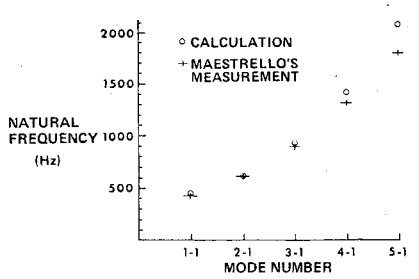

Fig. 4 Simple-panel natural frequencies.

Panel Idealization

The simple panel was idealized into an assembly of finite plate elements, 6 and 12 elements across the narrow and wide plate sides, respectively. This resulted in a structure represented by 72 equal-size plate elements and 91 nodes. All freedoms at the plate boundary were fully fixed, representing a clamped plate. Of the six freedoms at each node, only vertical out-of-plane displacement (55 freedoms) was retained in the analysis.

Natural frequencies for this panel idealization were calculated. The results are compared with measured results in Fig. 4. The mode numbers are the number of antinodes across the panel. The first number is for the flow direction and the second is for the direction normal to flow. These are the five modes that Maestrello identified down the centerline of the panel. Other modes, involving more than one antinode in the direction normal to flow, were calculated in this range of frequencies, but these were not seen experimentally because they have nodes on the panel centerline.

Response Solutions

Solutions for deflection response used Eqs. (10) and (13), a normal mode solution using only direct modes. The first 12 natural modes were retained in this analysis. The damping used in these solutions was determined from analyzing band widths between half-power points on response resonances determined from segmented, unpublished, high-resolution deflection PSD measurements supplied by Maestrello. This damping can be approximated by mass proportional damping as shown in Fig. 5.

Boundary-layer parameters used in simple panel solution analysis are as follows: $\langle p^2 \rangle = 4.07 \cdot 10^{-4}(\text{psi})^2$; $\delta^* = 0.155$ in.; $U_c = 0.88U = 6200$ in./sec; $M = 0.52$; $\theta = 9.1 \cdot 10^{-4}$ sec; $\xi_0 = 1.00$ in. (separation distance between node points); $\eta_0 = 1.167$ in.

These input parameters were used to generate the boundary-layer force co-PSD matrices. The rms pressure measured by Maestrello closely approximated $0.0072q$ (q is dynamic pressure) over the test Mach number range 0.14–0.78. Values selected for convection speed and eddy lifetime are characteristic of the frequency range of primary structural response. The first 3 modes were below 1200 Hz. Bull[20] shows that convection speeds for this lower-frequency range are greater than the mean eddy convection velocity of $0.80U$

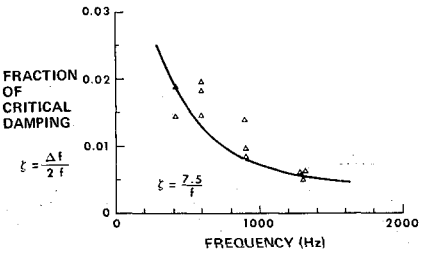

Fig. 5 Simple-panel damping.

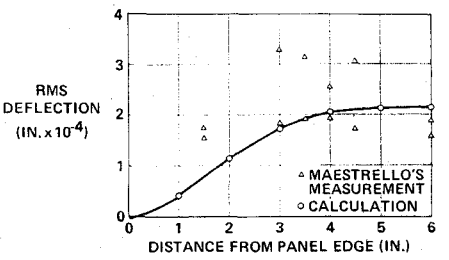

Fig. 6 Simple-panel rms deflection.

(U is the freestream speed). The value of $0.88U$ was chosen as more characteristic of the pressure loads that cause the structure to respond in the first 3 or 4 modes. Maestrello also shows that eddy lifetimes for these same lower-frequency pressure fluctuations are longer than mean eddy lifetime. Maestrello's narrow band measurements of eddy lifetimes for frequencies centered at 1200 Hz were used.

Calculated rms deflection and deflection PSD of the 0.080-in.-thick panel are compared with measured results in Figs. 6 and 7. Values of rms deflection are shown for points along the panel centerline. Maestrello made two determinations of the panel response at each location, as shown by the two sets of data points in Fig. 6.

Three of the points of Maestrello's deflection PSD measurement correspond exactly with the location points of calculated results.

A typical result for test point 4 is shown in Fig. 7. Deflection PSD was calculated for 33 frequencies, but some points are not shown because they fall below the graph. Maestrello's measured PSD has been corrected for bandwidth resolution errors, so that calculation and measurement can be compared on the same basis. Maestrello showed that half-power modal bandwidth was generally of the order of 15 Hz rather than the originally reported 40 Hz. The calculated 5-1 mode occurs at the upper end of the frequency scale, corresponding to the measured mode shown at 1815 Hz.

Comparison of analysis results with measurements shows good agreement. The rms deflection compares well near the panel center, with progressively increasing difference as the panel edge is approached. Variance in the two measurements at each location is considerable, reflecting the difficulty in measuring these low-level boundary-layer panel responses.

Significant errors occur in finite-element representations of continuous structure when the number of node points in a given direction is less than three per modal half-wavelength.

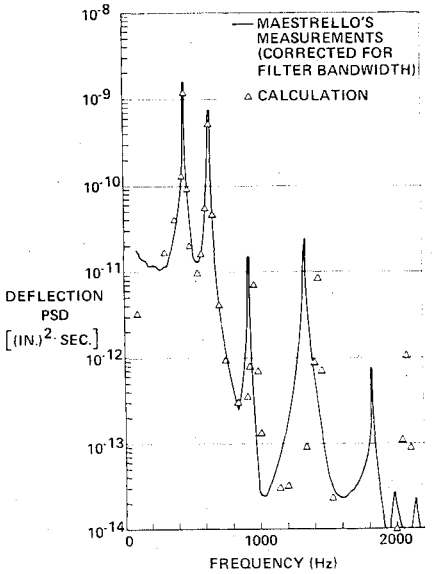

Fig. 7 Simple-panel deflection power spectrum.

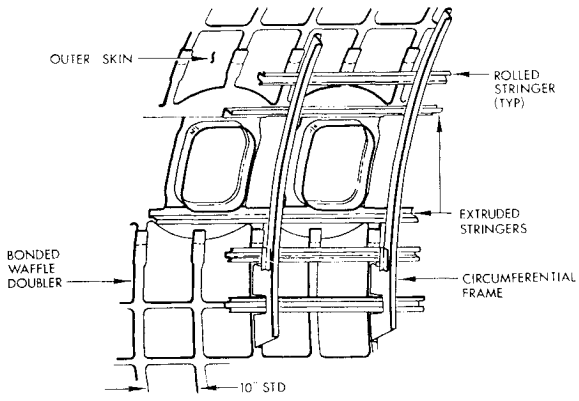

Fig. 8 Structure—window area.

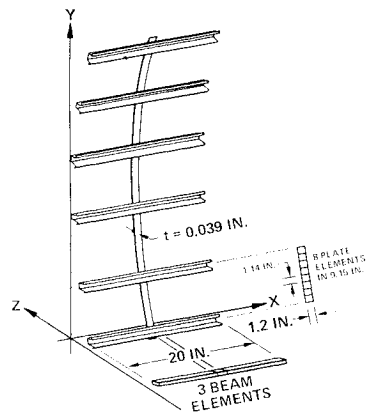

Fig. 9 Panel strip on stringers.

These errors are quite noticeable at the higher frequencies. Agreement between measured and calculated natural frequencies, shown in Fig. 4, is within 3.4% for the first three modes, and within 7.5% for the 4-1 mode. There are 2.2 structural nodes per half-wavelength for the 5-1 mode and the frequency error is 14%.

Aircraft Structures

Aircraft fuselage structure consists of a thin shell stiffened with stringers running fore and aft that are connected to circumferential frames. Tear straps, such as the system of waffle doublers shown in Fig. 8, are bonded to the skin to insure fail-safe design. The response of this complex system to turbulent boundary layers is examined by studying two simplifications: 1) a 6-stringer system attached to a 5-bay plate strip and 2) a skin-panel section between stringers and frames.

The panel-strip system is shown in Fig. 9. This structural system has been selected for a study of the response of multiple bays separated by stringers. The panel strip has no direct correspondence to multiple bays of skin panels attached to stringers and frames, but this model is a relatively small system that can be used to gain insight into the vibration of real aircraft structures.

The following questions are pertinent in a study of turbulent boundary-layer noise: 1) can the structure be treated as an assembly of individual panels acting statistically independent? 2) If not, how many of the panels are statistically dependent in their resonant response?

Additional questions are 1) how does boundary-layer thickness affect the size of the region of resonant statistical-dependent response? 2) what are the effects of curvature, cabin pressurization, and body flight loads on natural frequencies? The object of this study of the panel-strip system and the skin panel is to answer some of these questions.

Panel-Strip System

The finite-element idealization of the panel-strip system is also shown in Fig. 9. Three beam elements were used to represent the stringer: a short beam with length equal to the length of plate elements was attached to two longer beams with clamped supports at the ends. The beams were given both torsional and bending rigidity. The 0.039-in. thick, 48-in.-long panel strip was idealized by 42 flat plate elements. The beams and plates are made of aluminum alloy. Out-of-plane plate displacements were retained at 43 node points along one side of the panel strip. Mass for the plates and for only the center of the three beam elements was lumped at appropriate points among the 43 nodes.

Natural frequencies of the panel-strip system occurred in closely spaced groups of five, as shown in Fig. 10. There are 5 panel-strip bays, hence, the grouping in fives. This close grouping of modes in bands has been reported previously by Clarkson,[33] from measurements on an aft fuselage section, and by Lin,[34] from theoretical studies.

The lowest mode of each group of five is the stringer twisting mode, with adjacent bays out of phase, and the highest mode in each group is the stringer bending mode, with adjacent bays in phase. These modes, particularly for curved panels, have smaller frequency separation than Clarkson reported when he recommended that a design objective for sonic fatigue resistance should be to widely separate the frequency of these modes. The stringers actually bend very little because solutions for natural frequencies with no beam flexure allowed are identical within 1 Hz with frequencies calculated when beam flexure is permitted.

When the panel strip is curved with a radius of 74 in., the natural frequencies are increased and grouped more closely. The natural frequencies of the curved panels were substantially increased with the addition of uniform in-plane plate tension preloads of $N_x = 278$ lb/in. and $N_y = 555$ lb/in. in the x and circumferential directions, respectively. This load corresponds to 7.45 psig cabin pressurization. The first 6 natural modes for the curved and preloaded panel strip are shown in Fig. 11.

Solutions for panel-strip response to turbulent boundary layers are for a flight condition of Mach 0.78 at an altitude of 25,000 ft. Three boundary-layer displacement thicknesses of 0.418, 0.830, and 2.07 in., corresponding to airplane locations 340, 800, and 2500 in. aft of the nose, were considered. Conditions with flow, both parallel and normal to the stringers, were considered. Boundary-layer parameters used in panel-strip and waffled skin panel analysis are as follows:

x_e, in.	340	800	2500
$\langle p^2 \rangle$, psi^2	$1.56 \cdot 10^{-4}$	$1.13 \cdot 10^{-4}$	$0.71 \cdot 10^{-4}$
δ^*, in.	0.418	0.830	2.07

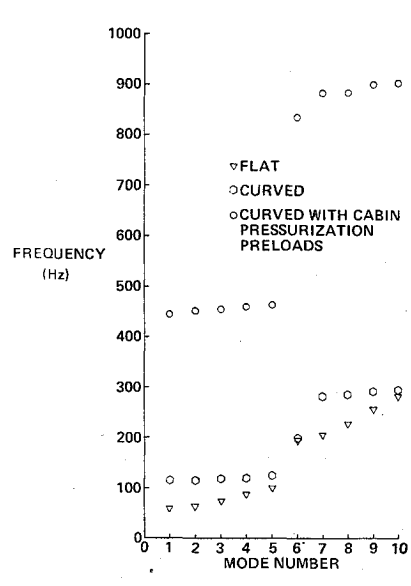

Fig. 10 Panel-strip natural frequencies.

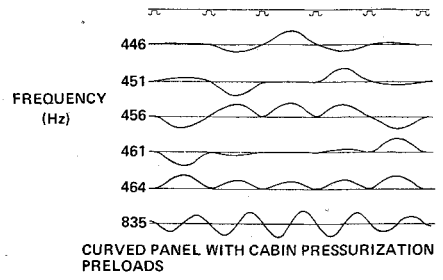

Fig. 11 Panel-strip modes.

The parameter x_e is the distance from the nose. The remaining parameters are the same for all locations: $U_c = 0.88U = 8371$ in./sec, $M = 0.78$ at 25,000-ft altitude, and $\theta = 2.6 \cdot 10^{-4}$ sec.

Typical deflection response of the panel strip is shown in Figs. 12 and 13. A mass proportional form of damping $\mu = 45$ was used. This is the value and form of damping found appropriate for skin-stringer panels by Jacobs and Lagerquist.[15] The first 10 natural modes were retained in these solutions, which neglected cross-modal coupling terms. The importance of cross terms [solution Eq (9)] was considered because the modes have very close frequency grouping. Admittance cross products were found to have values as high as 0.5 of the value of the direct terms. However, a solution using cross terms showed no increase in deflection or space correlation, indicating that the boundary-layer loading function did not excite this modal coupling.

Calculations for space correlation in Fig. 13 show that the resonant response of bays of the panel strip is statistically independent regardless of the direction of boundary-layer flow. The condition shown is for a displacement thickness of 0.418 in.; however, statistical independence of the panel bays was found for even the thickest boundary-layer displacement thicknesses. In fact, the deflection space correlation curves are practically identical for all three displacement thicknesses.

Waffled Skin Panel

The natural frequencies, normal modes, and turbulent boundary-layer loaded response of a section of skin structure were studied. The skin panel, shown in Fig. 14, is a typical section of aircraft skin structure located between adjacent frames and stringers. The skin panel is made from 0.036-in. aluminum alloy with a waffle pattern doubler bonded around the periphery and across the center. The grid lines show the finite-element idealization used to represent the panel. The idealization used 105 flat-plate elements assembled to represent both flat and curved panels. An average plate thickness was selected for each element in the regions near the doubler The out-of-plane displacement freedom was retained in the analysis at all interior (84) node points. The boundaries were clamped along the long direction and simply supported along the short side. Mass was lumped at node points with retained freedoms.

The natural frequencies of this waffled skin panel were determined on flat and curved skins of various thicknesses pre-

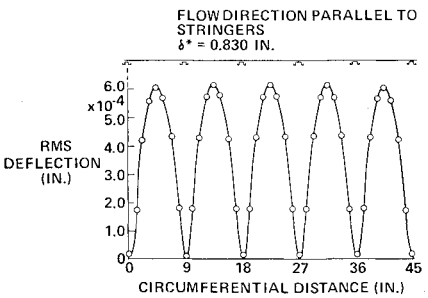

Fig. 12 Panel-strip rms deflection.

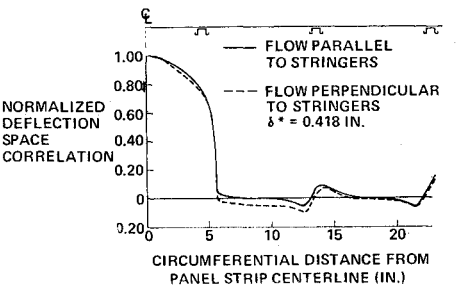

Fig. 13 Panel-strip deflection space correlation.

loaded by different combinations of cabin pressurization, body flight loads, and body ground loads. The first 5 natural frequencies for various combinations of these parameters are shown in Fig. 15. Table 1 summarizes the panel frequencies and mode shapes.

When the natural frequencies of flat and curved panels are compared, the order of occurrence of modes changes. The 1-1, 2-1, and 3-1 modes of the curved panel are ordered 3rd, 4th, and 5th, and the first 2 modes involve two half-wavelengths in the circumferential direction. This effect of curvature on the ordering of modes is similar to that shown by Arnold and Warburton[35] for cylindrical shells. With the application of in-plane tension preloads due to flight cabin pressurization, the ordering of modes again matches the mode order of the flat plate. The addition of ground and flight loads (due to mass, landing gear support, and tail balance loads) causes only slight changes of the natural frequencies, but the presence of in-plane shear loads distorts the classical panel modes, causing a loss of symmetry. Actually, the additional loads due to flight tend to have offsetting effects; the additional axial load N_x stiffens the panel, but the presence of the shearing load N_{xy} softens the panel.

When the waffle doublers are removed by making a constant 0.072-in.-thick curved and preloaded panel, the natural frequencies are actually reduced. The theoretical reasons for this phenomenon are discussed later.

The spacial scale of the random deflection of the waffled skin panel approximates the spacial scale previously discussed for the panel-strip system. Space correlation of panel deflections in both the x and y directions is shown in Fig. 16. These correlation plots are relative to a panel location centered as shown in the panel planview.

Boundary-Layer Thickness Effects

Boundary-layer thickness only slightly affects the rms displacement and spacial scale of the displacement response of typical aircraft structure. This is true even for a boundary-layer thickness characteristic of the aft cabin of large aircraft, as shown in Fig. 17. As the boundary-layer displacement thickness increases with distance from the nose, the rms fluctuating pressure decreases. The net effect is that the rms deflection of both the panel strip and waffled skin panel decreases slowly with distance aft. On the panel strip, response level is slightly larger when the flow is down the panel strip (y direction).

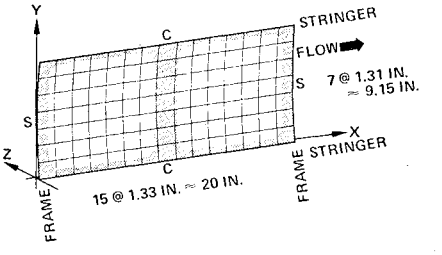

Fig. 14 Waffled skin panel.

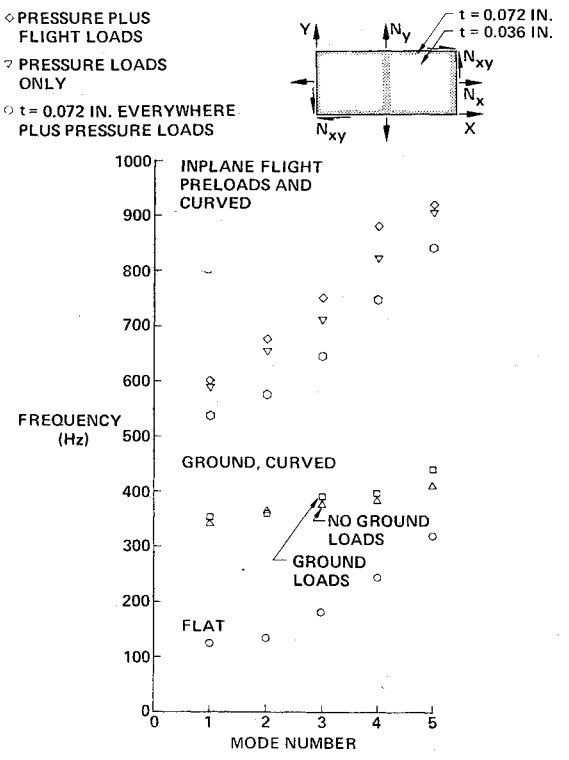

Fig. 15 Waffled-panel natural frequencies.

Higher-frequency modes were not considered and this must be remembered when interpreting these results. As the boundary layer becomes thinner, more power is distributed in the higher-frequency regions, and the errors arising from neglecting high-frequency modes will increase. However, as is shown in Fig. 18, the deflection PSD decreases with increasing frequency so that higher-frequency modes make only a small contribution to the total rms response. Summing the considerations, boundary-layer thickness changes are not expected to have large effects on structural deflection response.

Preload Effects

Figure 15 shows that increases in panel thickness can result in decreased natural frequencies of curved and preloaded panels. The explanation for this is that when constant in-plane preloads are applied to a panel, decreases in panel thickness can actually result in a stiffer panel. Fuller[36] and Hubbard and Houbolt[37] show that the natural frequencies of a classical, flat, simply supported panel with modes $\sin(m\pi x/a)\cdot\sin(n\pi y/b)$ that is subjected to in-plane loads N_x and N_y (positive, tension; negative, compression) are

$$f_{mn} = \frac{1}{2}\left[\frac{g}{\delta t}\left(N_x\frac{m^2}{a^2} + N_y\frac{n^2}{b^2}\right) + \frac{D\pi^2 g}{\gamma t}\left(\frac{m^2}{a^2} + \frac{n^2}{b^2}\right)^2\right]^{1/2} \tag{19}$$

Table 1 Waffled skin panel natural frequencies and modes

Symbol	Radius in.	Skin Thickness in.	Preloads lb/in. N_x	N_y	N_{xy}	Frequencies and Modes: Frequency Hz, Modes (m-n) *				
○	∞	0.036	---	---	---	124 (1-1)	135 (2-1)	182 (3-1)	245 (4-1)	323 (1-2)
△	74	0.036	---	---	---	343 (1-2)	368 (2-2)	379 (1-1)	387 (2-1)	414 (3-1)
□	74	0.036	47	---	-37	352 (1-2)	369 (2-2)	392 (1-1) ? (1-2)	397 (2-2) ? (2-1)	444 (3-1) ? (3-2)
○	74	0.072	278	555	---	540 (1-1)	578 (2-1)	647 (3-1)	750 (4-1)	843 (1-2)
▽	74	0.036	278	555	---	591 (1-1)	657 (2-1)	713 (3-1)	826 (4-1)	909 (1-2)
◇	74	0.036	378	555	-60	599 (1-1)	679 (2-1)	751 (3-1)	885 (4-1) ? (4-2)	922 (1-2)

* Mode numbers m and n in the x and y directions respectively.

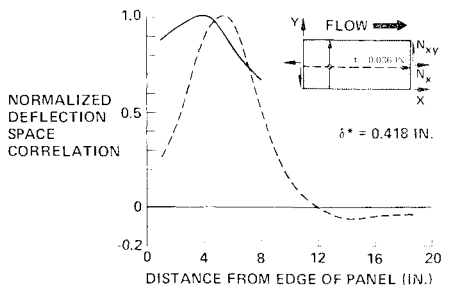

Fig. 16 Waffled-panel deflection space correlation.

where $D = Et^3/12(1-\nu^2)$, g is the acceleration of gravity, γ is panel density, E is the modulus of elasticity, ν is Poisson's ratio, and a and b are the panel length and width, respectively. The remaining terms have previously been defined. This function has an extremal value at thickness t_1

$$t_1 = \left\{\frac{6(1-\nu^2)}{E\pi^2}\cdot\frac{[N_x(m^2/a^2) + N_y(n^2/b^2)]}{[(m^2/a^2) + (n^2/b^2)]^2}\right\}^{1/3} \tag{20}$$

A plot of Eq. (19) is shown in Fig. 19 for typical modes 1-1 and 10-4. The panel size and preload values due to cabin pressurization are shown. The panel thickness that resulted in minimum natural frequency was calculated using Eq. (20). This explains why the natural frequencies of the waffled skin panel decreased with an increase in thickness.

Conclusions

The boundary-layer loading function developed and used in this report shows how random loadings with very small spacial scale can be adequately represented for a finite-element system when structural element size exceeds the spacial scale of the loading. Applications of this boundary-layer loading function with a finite-element random-vibration analysis system to determine the deflection response of a simple clamped plate show excellent agreement with measurements. The study of a structural panel-strip system shows that even for thick boundary layers, the lower-frequency resonant deflection response of individual panel bays is statistically independent. This leads to the conclusion that the low-frequency response of an aircraft structure to turbulent boundary layers can be adequately described by calculating the response of single-skin panels, treating an assembly of skin panels as statistically independent. Curvature and in-plane preloads due to differential cabin pressurization substantially stiffen a structure, raising low-order natural frequencies and causing the grouping of natural frequencies to be more dense. Adding thickness to a skin panel preloaded by cabin pressurization does not always result in increased natural frequencies. Boundary-layer thickness changes on typical aircraft do not substantially affect deflection response in the lower-frequency modes.

Appendix: Force Cross-PSD Matrix Elements

Force cross-PSD on element pairs has been determined by evaluation of the integral in Eq. (18), where Eq. (17) has been

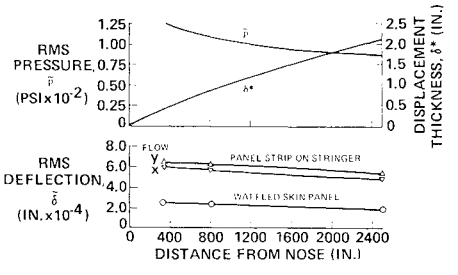

Fig. 17 Fuselage displacement response.

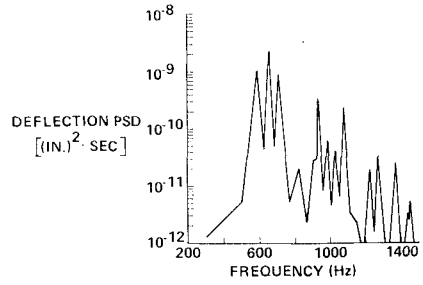

Fig. 18 Typical waffled-panel displaceent power spectrum.

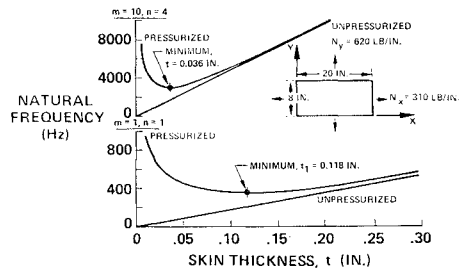

Fig. 19 Preload and thickness effects on natural frequencies.

used to define the pressure cross-PSD. The results of this evaluation are summarized here.

Node points are assumed to lie on the intersection of a repetitive grid. Then separation distances are integer multiples of basic x and y direction separation distances ξ_0 and η_0. For node points i and j, $\xi = n_{ij}\xi_0$ and $\eta = m_{ij}\eta_0$, where $n_{ij} = (x_j - x_i)/\xi_0$ and $m_{ij} = (y_j - y_i)/\eta_0$. The use of integer multiples of the basic separation distance has been introduced to take advantage of the homogeneous nature of fluctuating pressures in the turbulent boundary layer. The full matrix of terms can then be constructed from a small set of components dependent only on n_{ij} and m_{ij}. This makes large savings on computing time.

Final equations for the power and cross-power spectral density of forces acting on node points of a structure are

force PSD: $(i = j)$, $(n_{ij} = m_{ij} = 0)$

$$C_{Fii}(\omega) = \hat{K}'\hat{P}\hat{\Phi} \tag{A1}$$

$$Q_{Fii}(\omega) = 0 \tag{A2}$$

force cross-PSD: $(i \neq j)$

$(n_{ij} = 0, m_{ij} \neq 0)$

$$C_{Fij}(\omega) = \hat{K}'\hat{P}\hat{\Phi} \tag{A3}$$

$$Q_{Fij}(\omega) = 0 \tag{A4}$$

$(n_{ij} \neq 0, m_{ij} \neq 0)$

$$C_{Fij}(\omega) = \hat{K}'\hat{C}\hat{\Phi} \tag{A5}$$

$$Q_{Fij}(\omega) = \hat{K}'\hat{Q}\hat{\Phi}\exp(-|n_{ij}a\xi_0|) \tag{A6}$$

Since the force cross-PSD matrices are hermitian, the real part is symmetric, and the imaginary part is skew symmetric. So, for each term defined previously, the following relations hold: $C_{Fji}(\omega) = C_{Fij}(\omega)$ and $Q_{Fji}(\omega) = -Q_{Fij}(\omega)$.

The term $\hat{K}'$ is a constant

$$\hat{K}' = \langle p^2\rangle\eta_0/3.34U_cB^2 \tag{A7}$$

The power spectral density's dependence on ξ_0 is

$$\hat{P}(\omega) = 2/(a^2 + b^2)^2a\{\xi_0(a^2 + b^2) + (b^2 - a^2)[1 - \exp(-a\xi_0)\cos(b\xi_0)] - 2ab\exp(-a\xi_0)\sin(b\xi_0)\} \tag{A8}$$

The term $\hat{\Phi}$ defines dependence on η and is evaluated as a numerical integration,

$$\hat{\Phi}(\omega) = \frac{B}{2\eta_0}\sum_{n=1}^{3} A_nK_nZ_n(m_{ij},\omega) \tag{A9}$$

$$Z_n(m_{ij},\omega) = \int_{-\eta_0/2}^{\eta_0/2}\int_{-\eta_0/2}^{\eta_0/2} I_n d\eta_j d\eta_i \tag{A10}$$

$$I_n = \frac{\exp\{-(\omega/BU_c)[K_n^2 + B^2(m_{ij}\eta_0 + \eta_j - \eta_i)^2]^{1/2}\}}{[K_n^2 + B^2(m_{ij}\eta_0 + \eta_j - \eta_i)^2]^{1/2}} \tag{A11}$$

The terms $\hat{C}$ and $\hat{Q}$ are those parts of Eq. (18) with dependence on ξ:

$$\begin{Bmatrix}\hat{C}\\ \hat{Q}\end{Bmatrix} = \frac{4}{(a^2 + b^2)^2}\begin{bmatrix}V & W\\ W & -V\end{bmatrix}\begin{Bmatrix}\cos(n_{ij}b\xi_0)\\ \sin(n_{ij}b\xi_0)\end{Bmatrix} \tag{A12}$$

$$V = ab\sin(b\xi_0)\sinh(a\xi_0) + [(b^2 - a^2)/2][1 - \cos(b\xi_0)\cosh(a\xi_0)] \tag{A13}$$

$$W = [(a^2 - b^2)/2]\sin(b\xi_0)\sinh(a\xi_0) + ab[1 - \cos(b\xi_0)\cosh(a\xi_0)] \tag{A14}$$

where $a = 1/U_c\theta$, $b = \omega/U_c$.

The force co-PSD and quad-PSD matrices are each constructed separately from these equations. Equations (A8), (A13), and (A14) differ from those previously defined.[11] When these corrected equations were used in solution analysis, the changes in the simple-panel response reported in that analysis were insignificant.

References

[1] Powell, A., "On the Fatigue Failure of Structures Due to Vibrations Excited by Random Pressure Fields," *The Journal of the Acoustical Society of America*, Vol. 30, 1958, p. 1130.

[2] Eringen, A. C., "Response of Beams and Plates to Random Loads," *Journal of Applied Mechanics*, Vol. 24, 1957, p. 46.

[3] Lyon, R. H., "Response of Strings to Random Noise Fields," *The Journal of the Acoustical Society of America*, Vol. 28, 1956, p. 391.

[4] Thomson, W. T. and Barton, M. V., "The Response of Mechanical Systems to Random Excitation," *Journal to Applied Mechanics*, Vol. 24, June 1957, pp. 248–251.

[5] Dyer, I., "Boundary Layer Induced Flow Noise," *The Journal of the Acoustical Society of America*, Vol. 31, 1959, p. 1566.

[6] Wilby, J. F., "The Response of Simple Panels to Turbulent Boundary Layer Excitation," AFFDL-TR-67-70, 1967, Air Force Flight Dynamics Lab., Wright-Patterson Air Force Base, Ohio.

[7] Trubert, M. R. P., "Response of Elastic Structures to Statistically Correlated Multiple Random Excitations," *The Journal of the Acoustical Society of America*, Vol. 35, 1963, p. 1009.

[8] Fuller, J. R. and Newsom, C. D., "A Theoretical Approach for Determining the Response of Complex Structure to Arbitrary Random Noise Fields," D6-6897TN, 1965, The Boeing Co., Renton, Wash.

[9] Newsom, C. D., "Response of Multi-Degree-of-Freedom Systems to Random Excitation Using Finite Element Theory," D6-15745TN, 1967, The Boeing Co., Renton, Wash.

[10] Newsom, C. D., Fuller, J. R., and Sherrer, R. E., "A Finite Element Approach for the Analysis of Randomly Excited Complex Elastic Structures," presented at the AIAA/ASME 8th Structures, Structural Dynamics, and Materials Conference, Palm Springs, Calif., March 29, 1967.

[11] Jacobs, L. D. and Lagerquist, D. R., "A Finite-Element Analysis of Simple Panel Response to Turbulent Boundary Layers," AFFDL-TR-67-81, 1968, Air Force Flight Dynamics Lab., Wright-Patterson Air Force Base, Ohio.

[12] Hurty, W. C. and Rubinstein, M. F., *Dynamics of Structures*, Prentice-Hall, Englewood Cliffs, N. J., 1964.

[13] Lagerquist, D. R. and Jacobs, L. D., "Random-Vibration Analysis System for Complex Structures, Part I, Engineering User's Guide," AFFDL-TR-68-43, Part I, 1968, Air Force Flight Dynamics Lab., Wright-Patterson Air Force Base, Ohio.

[14] Tsurusaki, K. and Wallace, F. S., "Random-Vibration Analysis System for Complex Structures, Part II, Computer Program Description," AFFDL-TR-68-43, Part II, 1968, Air Force Flight Dynamics Lab., Wright-Patterson Air Force Base, Ohio.

[15] Jacobs, L. D. and Lagerquist, D. R., "Finite-Element Analysis of Complex Panel Response to Random Loads," AFFDL-TR-68-44, 1968, Air Force Flight Dynamics Lab., Wright-Patterson Air Force Base, Ohio.

[16] Maestrello, L., "Measurement and Analysis of the Response Field of Turbulent Boundary Layer Excited Panels," *Journal of Sound and Vibration*, Vol. 2, 1965, p. 270.

[17] Maestrello, L., "Design Criterion of Panel Structure Excited by Turbulent Boundary Layer," *Journal of Aircraft*, Vol. 5, No. 3, May–June 1968, p. 321.

[18] Maestrello, L., "Boundary Layer Pressure Fluctuations on the 707 Prototype Airplane," paper presented at the 65th Meeting of the Acoustical Society of America, Seattle, Wash., Nov. 7–10, 1962.

[19] Maestrello, L., "Radiation from and Panel Response to a Supersonic Turbulent Boundary Layer," D1-82-0719, 1968, The Boeing Co., Seattle, Wash.

[20] Bull, M. K., Wilby, J. F., and Blackman, D. R., "Wall Pressure Fluctuations in Boundary Layer Flow and Response of Simple Structures to Random Pressure Fields," AASU Rept. 243, 1963, Univ. of Southampton, England.

[21] Hodgson, T. H., "Pressure Fluctuation in Shear Flow Turbulence," College Aero Note 129, 1962, College of Aeronautics, Cranfield, Bletchley, Bucks, England.

[22] Mayes, W. H., Hilton, D. A., and Hardesty, C. A., "In-Flight Noise Measurements of Three Project Mercury Vehicles," TN D-997, 1962, NASA.

[23] Wiley, D. R. and Seidl, M. G., "Aerodynamic Noise Tests on X-20 Scale Models," AFFDL-TR-65-192, 1965, Air Force Flight Dynamics Lab., Wright-Patterson Air Force Base, Ohio.

[24] Harrison, M., "Pressure Fluctuations on the Wall Adjacent to a Turbulent Boundary Layer," Rept. 1260, 1958, David Taylor Model Basin, Washington, D. C.

[25] Willmarth, W. W. and Wooldridge, C. E., "Measurements of the Fluctuating Pressure Beneath a Thick Turbulent Boundary Layer," 1962, Univ. of Michigan, College of Engineering, Ann Arbor, Mich.

[26] Kistler, A. L. and Chen, W. S., "The Fluctuating Pressure Field in a Supersonic Turbulent Boundary Layer," JPL-TR-32-277, 1962, Jet Propulsion Lab., Pasadena, Calif.

[27] Serafini, J. S., "Wall-Pressure Fluctuations and Pressure-Velocity Correlations in a Turbulent Boundary Layer," TRR-165, 1963, NASA.

[28] Jacobs, L. D., Young, M. C., and Tsurusaki, K., "A Computer Program on Turbulent Boundary Layer Loads for use with Finite-Element Structural Analysis Systems," D6-23769, May 1969, The Boeing Co., Renton, Wash.

[29] Khinchine, A. I., *Mathematical Foundations of Statistical Mechanics*, Dover, New York, 1949.

[30] Davenport, W. B. and Root, W. L., *An Introduction to the Theory of Random Signals and Noise*, McGraw-Hill, New York, 1958.

[31] Bendat, J. S., *Principles and Applications of Random Noise Theory*, Wiley, New York, 1958.

[32] Hinze, J. O., *Turbulence, An Introduction to Its Mechanism and Theory*, McGraw-Hill, New York, 1959.

[33] Clarkson, B. L., "The Design of Structure to Resist Jet Noise Fatigue," *Journal of the Royal Aeronautical Society*, Vol. 66, 1962, p. 603.

[34] Lin, Y. K., "Free Vibration of Continuous Skin Stringer Panels," *Journal of Applied Mechanics*, Dec. 1960.

[35] Arnold, R. N. and Warburton, G. B., "The Flexural Vibration of Thin Cylinders," *Proceedings of the Institute of Mechanical Engineers*, Vol. A, 1963, p. 167.

[36] Fuller, J. R., "A Theoretical Approach for the Determination of Acoustic Transmission Losses Through Loaded Rectangular Skin Panels," D6-7606TN, 1964, The Boeing Co., Renton, Wash.

[37] Hubbard, H. H. and Houbolt, J. C., "Vibration Induced by Acoustic Waves," Chapter 48 in *Shock and Vibration Handbook*, edited by C. M. Harris and C. E. Crede, Vol. 3, McGraw-Hill, 1961.